THE JOURNAL OF PHYSICAL CHEMISTRY C
A JOURNAL OF THE AMERICAN CHEMICAL SOCIETY

pubs.acs.org/JPCC

Feature Article

Thermodynamic Analysis and Interpretative Guide to Entropic Potential Measurements of Lithium-Ion Battery Electrodes

Sun Woong Baek, Muna Saber, Anton Van der Ven,* and Laurent Pilon*

Cite This: *J. Phys. Chem. C* 2022, 126, 6096−6110

Read Online

ACCESS | Metrics & More | Article Recommendations | Supporting Information

ABSTRACT: This paper reviews and clarifies the fundamental thermodynamic relationships relevant to the interpretation of potentiometric entropy measurements on lithium-ion batteries to gain insight into the physicochemical phenomena occurring during cycling. First, contributions from configurational, vibrational, and electronic excitations to the entropy of an *ideal* intercalation compound used as a cathode in a battery system are analyzed. The results of this analysis are used to provide an interpretative guide of open circuit voltage $U_{ocv}(x,T)$ and entropic potential $\partial U_{ocv}(x,T)/\partial T$ measurements to identify different mechanisms of intercalation, including (i) lithium intercalation as a homogeneous solid solution, (ii) ion ordering reactions from a homogeneous solid solution, (iii) first-order phase transitions involving a two-phase coexistence, and/or (iv) first-order phase transitions passing through a stable intermediate phase. These interpretations illustrated with experimental data for different battery electrode materials including TiS_2, $LiCoO_2$, $Li_{4/3}Ti_{5/3}O_4$, $LiFePO_4$, and graphite electrodes with metallic lithium as the counter electrode. The systematic interpretation of $U_{ocv}(x,T)$ and $\partial U_{ocv}(x,T)/\partial T$ can enhance other structural analysis techniques such as X-ray diffraction, electron energy-loss spectroscopy, and Raman spectroscopy. The thermodynamic analysis and the interpretive guide will be instrumental in the discovery of new battery materials.

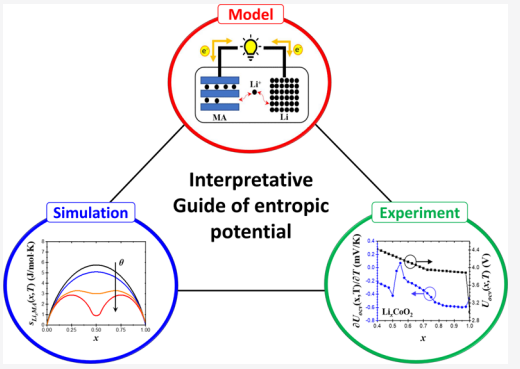

1. INTRODUCTION

With the increasing demand for portable electronic devices and electric vehicles, tremendous efforts have been devoted to improving the energy and power densities, life span, and safety of electrical energy storage systems.[1−5] In this context, lithium-ion batteries (LIBs) have received particular attention for their high energy density and relatively low environmental impact.[6] Improving the performance of LIBs can be achieved not only by cell engineering but also with the discovery of new electrode materials.[7,8] The latter typically undergo dramatic changes in lattice structure upon the insertion/deinsertion of Li^+ ions. Some materials, such as TiS_2, maintain their crystal structure and form a homogeneous solid solution upon lithiation.[9] Other materials undergo phase transitions during Li insertion and removal. $FePO_4$, for example, undergoes a first-order phase transition from $FePO_4$ to $LiFePO_4$, resulting in the coexistence of these two phases during lithiation.[10] Graphite, in contrast, forms a stable intermediate phase during a first-order phase transition, resulting in two separate two-phase coexistence regions including one between LiC_{24} and LiC_{12} and the other between LiC_{12} and LiC_6.[11]

Over the past few decades, a number of analytical devices and techniques, including *in situ* X-ray diffraction (XRD),[12−15] *ex situ* electron microscopy,[16−18] electron energy-loss spectroscopy (EELS),[19] and Raman spectroscopy[20−22] have been developed to investigate changes in the crystal structure of battery electrode materials during cycling. However, in order to use such analytical methods, expensive equipment and time-consuming sample preparation may be required. Alternatively, the entropy measurement technique is a simple *operando* method performed on coin cells using a conventional potentiostat.[23]

Several entropy measurement techniques for battery systems have been developed, including (i) potentiometric entropy measurements,[24] (ii) electrothermal impedance spectroscopy,[25] and (iii) sinusoidal temperature oscillation entropymetry.[26] These methods aim to measure the derivative of the open circuit voltage $U_{ocv}(x,T)$ with respect to temperature T for a given lithium composition x, i.e., $\partial U_{ocv}(x,T)/\partial T$, also known as the entropic potential. While significant progress has been made in measuring $\partial U_{ocv}(x,T)/\partial T$, its interpretation remains ambiguous.[24−30] In particular, it remains unclear as to how characteristic features in the $\partial U_{ocv}(x,T)/\partial T$ curve as a function of x are to be correlated with the occurrence of solid

Received: December 9, 2021
Revised: March 11, 2022
Published: April 1, 2022

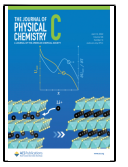

Downloaded via UNIV OF CALIFORNIA LOS ANGELES on April 14, 2022 at 08:00:51 (UTC).
See https://pubs.acs.org/sharingguidelines for options on how to legitimately share published articles.

© 2022 American Chemical Society

https://doi.org/10.1021/acs.jpcc.1c10414
J. Phys. Chem. C 2022, 126, 6096−6110

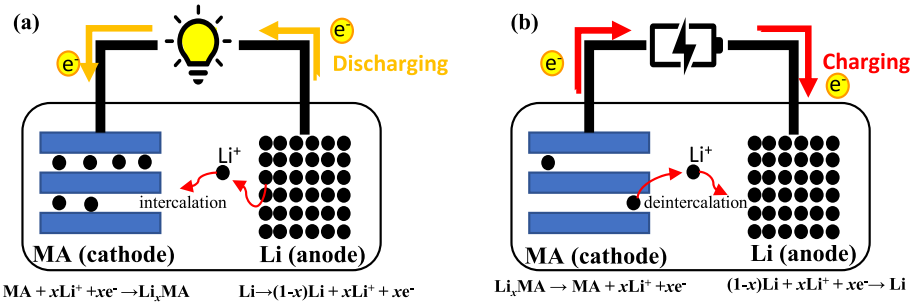

Figure 1. Schematic of the ionic and electronic transport processes in a lithium-ion battery and redox reactions associated with the (a) *discharging* and (b) *charging* processes.

solutions, order−disorder phenomena, and first-order phase transformations within the electrode materials. There is, therefore, a scientific need to revisit the interpretation of entropic potential measurements to deepen our understanding of physicochemical phenomena occurring in a battery system.

This paper aims to review and clarify fundamental thermodynamic relationships in order to develop an interpretative guide to $U_{ocv}(x,T)$ and $\partial U_{ocv}(x,T)/\partial T$ *operando* measurements so as to gain insights into the different physicochemical phenomena occurring in LIBs under different charging/discharging scenarios. Phenomena of interest include intercalation in homogeneous solid solutions, cation ordering, first-order phase transitions accompanied by two-phase coexistence, and first-order transitions with an intermediate phase. The thermodynamic relationships are rigorously derived and systematically illustrated with experimental data for various LIB materials. The analysis starts with a rigorous treatment of *ideal* intercalation compounds, which capture the first-order contributions to $U_{ocv}(x,T)$ and $\partial U_{ocv}(x,T)/\partial T$ due to configurational, vibrational and electronic excitations. Deviations from ideality are then discussed in the context of experimentally measured $U_{ocv}(x,T)$ and $\partial U_{ocv}(x,T)/\partial T$ curves of important intercalation compounds.

2. ANALYSIS

2.1. Cell Open-Circuit Voltage and Entropic Potential.

Figure 1a and 1b show a typical LIB consisting of a metallic intercalation compound MA serving as the cathode, a lithium metal electrode serving as the anode, and a Li-ion based electrolyte. The intercalation compound MA consists of a transition metal M and an anion unit referred to as A. Figure 1a schematically shows the direction of ion and electron transport in a LIB during *discharging*. Then, the Li^+-ions intercalate into MA, the electrochemically active material of the cathode, to balance the charge of electrons coming from the oxidation of the metallic lithium anode according to[31,32]

$$\mathrm{Li} \rightarrow (1-x)\mathrm{Li} + x\mathrm{Li}^+ + x\mathrm{e}^- \tag{1}$$

Upon insertion of Li^+ ions in the cathode, MA transforms into a lithiated compound Li_xMA, according to[31,32]

$$\mathrm{MA} + x\mathrm{Li}^+ + x\mathrm{e}^- \rightarrow \mathrm{Li}_x\mathrm{MA} \tag{2}$$

The lithium composition x is defined as the fraction of the number of intercalated lithium N_{Li} per number of host MA units N_{MA}, i.e.,

$$x = \frac{N_{\mathrm{Li}}}{N_{\mathrm{MA}}} \tag{3}$$

Combining eqs 1 and 2 yields the overall reaction of the battery system during *discharging*[31,32]

$$\mathrm{MA} + \mathrm{Li} \rightarrow \mathrm{Li}_x\mathrm{MA} + (1-x)\mathrm{Li} \tag{4}$$

The arrows in the above reactions are reversed during *charging*, as schematically illustrated in Figure 1b.

Variations in the lithium composition x of the cathode material during *charging*/*discharging* leads to a change in the open circuit voltage of the battery. The open circuit voltage $U_{ocv}(x,T)$ of a Li^+ ion battery is related to fundamental thermodynamic quantities of the electrodes according to the Nernst equation[33]

$$U_{ocv}(x,\,T) = -\frac{\mu_{\mathrm{Li}}^{\mathrm{Li}_x\mathrm{MA}}(x,\,T) - \mu_{\mathrm{Li}}^{\circ}(T)}{e} \tag{5}$$

where e is the elementary charge while $\mu_{\mathrm{Li}}^{\mathrm{Li}_x\mathrm{MA}}(x,T)$ and $\mu_{\mathrm{Li}}^{\circ}(T)$ are respectively the Li chemical potentials of Li_xMA in the cathode and of metallic Li in the anode. The lithium chemical potential $\mu_{\mathrm{Li}}^{\mathrm{Li}_x\mathrm{MA}}(x,T)$ of Li_xMA is related to the Gibbs free energy of Li_xMA according to

$$\mu_{\mathrm{Li}}^{\mathrm{Li}_x\mathrm{MA}}(x,\,T) = \frac{\partial G_{\mathrm{Li}_x\mathrm{MA}}(x,\,T)}{\partial N_{\mathrm{Li}}} = \left(\frac{\partial g_{\mathrm{Li}_x\mathrm{MA}}(x,\,T)N_{\mathrm{MA}}}{\partial x}\right)\left(\frac{\partial x}{\partial N_{\mathrm{Li}}}\right) = \frac{\partial g_{\mathrm{Li}_x\mathrm{MA}}(x,\,T)}{\partial x} \tag{6}$$

where $g_{Li_xMA}(x,T)$ is the Gibbs free energy of Li_xMA normalized by the number N_{MA} of MA units. Furthermore, the chemical potential of Li in the anode can be expressed as

$$\mu_{\mathrm{Li}}^{\circ}(T) = \frac{\partial G_{\mathrm{Li}}(T)}{\partial N_{\mathrm{Li}}} = \frac{G_{\mathrm{Li}}(T)}{N_{\mathrm{Li}}} = g_{\mathrm{Li}}^{\circ}(T) \tag{7}$$

where the middle equality holds because the anode is a pure Li metal, i.e., a single component solid. Here, eq 7 assumes that the metallic Li electrode has macroscopic dimensions and that contributions from surface energy can be neglected.[34] In this thermodynamic limit, the Li chemical potential of the anode is a constant under isothermal and isobaric conditions.

By substituting eqs 6 and 7 into eq 5, the open circuit voltage $U_{ocv}(x,T)$ of the battery can be related to the Gibbs free energies of the two electrodes as

https://doi.org/10.1021/acs.jpcc.1c10414
J. Phys. Chem. C 2022, 126, 6096−6110

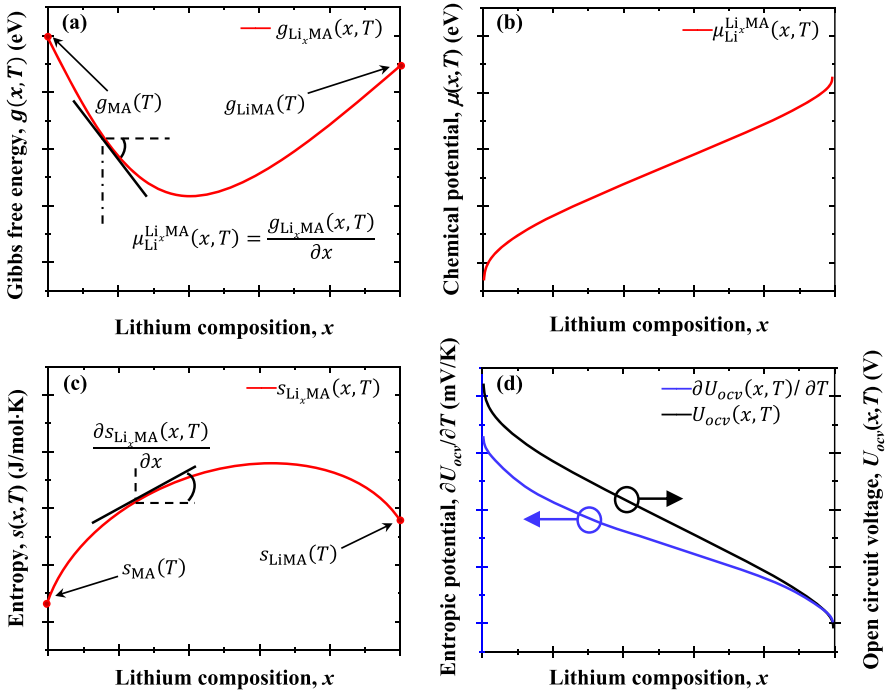

Figure 2. (a) Schematic plots of Gibbs free energy $g_{Li_xMA}(x,T)$, (b) chemical potential $\mu_{Li}^{Li_xMA}(x,T)$, (c) entropy $s_{Li_xMA}(x,T)$ of Li_xMA, and (d) open circuit voltage $U_{ocv}(x,T)$ and entropic potential $\partial U_{ocv}(x,T)/\partial T$ of the battery cell as functions of lithium composition x at temperature T when MA forms a homogeneous solid solution upon lithiation.

$$U_{ocv}(x,\ T) = -\frac{1}{e}\left[\frac{\partial g_{Li_xMA}(x,\ T)}{\partial x} - g_{Li}^{\circ}(T)\right] \tag{8}$$

Based on Clairaut's theorem, taking the derivative of both sides of eq 8 with respect to temperature T yields

$$\frac{\partial U_{ocv}(x,\ T)}{\partial T} = -\frac{1}{e}\left[\frac{\partial}{\partial x}\left(\frac{\partial g_{Li_xMA}(x,\ T)}{\partial T}\right) - \frac{\partial g_{Li}^{\circ}(T)}{\partial T}\right] \tag{9}$$

The temperature derivative of the Gibbs free energy, under isobaric conditions, is related to the entropy $s(x,T)$ according to[35]

$$s(x,\ T) = -\frac{\partial g(x,\ T)}{\partial T} \tag{10}$$

where both $s(x,T)$ and $g(x,T)$ are normalized per unit of MA or metallic Li. Thus, it is possible to relate the temperature derivative of the open circuit voltage to the entropies of the cathode material and the Li anode according to

$$\frac{\partial U_{ocv}(x,\ T)}{\partial T} = \frac{1}{e}\left[\frac{\partial s_{Li_xMA}(x,\ T)}{\partial x} - s_{Li}^{\circ}(T)\right] \tag{11}$$

The partial derivative $\partial s_{Li_xMA}(x,T)/\partial x$ with respect to lithium composition x of the entropy of the cathode $s_{Li_xMA}(x,T)$ per unit MA of Li_xMA is referred to as the partial entropy. Note that $s_{Li}^{\circ}(T)$ is the entropy of the metallic lithium electrode which is always positive and depends only on temperature; at room temperature $s_{Li}^{\circ}(298K)$ was reported to be 29 J/mol·K.[36]

In the following sections, we qualitatively analyze how the open circuit voltage $U_{ocv}(x,T)$ and the entropic potential $\partial U_{ocv}(x,T)/\partial T$ behave for intercalation compounds that (i) intercalate Li as a homogeneous solid solution, (ii) undergo ion ordering upon intercalation, (iii) undergo a first-order phase transition involving a two-phase coexistence, and (iv) exhibit a series of first-order phase transitions with stable intermediate phases. These interpretations were illustrated with experimental data collected for this study for different battery electrode materials including TiS_2, $LiCoO_2$, $Li_{4/3}Ti_{5/3}O_4$, $LiFePO_4$ and graphite electrodes with metallic lithium as the counter electrode. Here, $U_{ocv}(x,T)$ and $\partial U_{ocv}(x,T)/\partial T$ of TiS_2, $LiCoO_2$, and graphite electrodes were measured with the custom-made setup described in ref 23 and in the Supporting Information, along with the experimental procedure. However, measurements for $U_{ocv}(x,T)$ and $\partial U_{ocv}(x,T)/\partial T$ for cells consisting of $Li_xTi_{5/3}O_4$[37] and Li_xFePO_4[10] electrodes and metallic lithium counter electrode were obtained from previous studies.

2.2. Intercalation in Homogeneous Solid Solution.

2.2.1. Introduction. Layered materials such as TiS_2[9] and $LiCoO_2$[12,38] have been widely investigated as Li-ion battery electrode materials. They form homogeneous solid solutions and maintain their crystal structure over large intervals of Li concentration. These layered materials consist of a stacking of two-dimensional transition metal sulfide or oxide sheets that are held together by van der Waals forces in the absence of Li.[39,40] Li^+ ions can intercalate into the vacant sites between the two-dimensional sheets of the host. The Gibbs free energy $g_{Li_xMA}(x,T)$ of an intercalation compound Li_xMA that forms a homogeneous solid solution upon lithiation is a convex function with respect to the lithium composition x as schematically illustrated in Figure 2a. In addition, Figure 2b illustrates that the lithium chemical potential $\mu_{Li}^{Li_xMA}(x,T)$ of Li_xMA monotonically decreases with increasing lithium composition x for a homogeneous solid solution. Figure 2c schematically plots the entropy $s_{Li_xMA}(x,T)$ of Li_xMA as a

https://doi.org/10.1021/acs.jpcc.1c10414
J. Phys. Chem. C 2022, 126, 6096−6110

function of the Li composition. For a solid solution, $s_{Li_xMA}(x,T)$ is a concave function with respect to the lithium composition x. Finally, Figure 2d plots the open circuit voltage $U_{ocv}(x,T)$ and the entropic potential $\partial U_{ocv}(x,T)/\partial T$ of the battery for a host material MA that forms a homogeneous solid solution during Li insertion. Overall, lithium intercalation in a homogeneous solid solution is characterized by a monotonically decreasing $U_{ocv}(x,T)$ and $\partial U_{ocv}(x,T)/\partial T$ with lithium composition x.

The insertion of Li into Li_xMA alters a variety of properties of the host material, including its lattice parameters, electronic structure, and vibrational frequencies. In general, Li ions within the host also interact with other Li ions, with the strength and nature of these interactions determining whether the intercalation compound favors a solid solution, a series of ordered phases, or a state of two-phase coexistence. Before considering real intercalation compounds where such interactions are present, important insights can be generated by studying the electrochemical properties of *ideal* intercalation compounds, defined as compounds in which interactions among Li ions and between Li and the host can be neglected. An *ideal* intercalation compound serves as a useful model to obtain bounds and to identify first-order trends of various thermodynamic quantities.

The Gibbs free energy of a solid arises from a variety of electronic and atomic excitations. There are three important sources of the Gibbs free energy in an intercalation compound.[41,42] One emerges from configurational degrees of freedom associated with all possible ways of arranging Li ions and vacancies over the interstitial sites of the intercalation compound.[43] A second contribution arises from vibrational excitations involving both the host ions and the Li ions.[44] A third is due to electronic excitations, assuming a variety of forms, as described later. While it is generally not possible to disentangle these contributions for real solids, for *ideal* intercalation compounds, it is possible to express the total Gibbs free energy of an *ideal* intercalation compound as a simple sum of these three contributions, i.e.,

$$g(x,\,T) = g^{conf}(x,\,T) + g^{vib}(x,\,T) + g^{elec}(x,\,T) \qquad (12)$$

where $g^{conf}(x,T)$, $g^{vib}(x,T)$, and $g^{elec}(x,T)$ are the configurational, vibrational, and electronic Gibbs free energies, respectively, of the compound. Based on eq 10, the entropy can also be expressed as the sum of individual contributions according to

$$s(x,\,T) = s^{conf}(x,\,T) + s^{vib}(x,\,T) + s^{elec}(x,\,T) \qquad (13)$$

The following sections derive expressions for the entropy of an ideal intercalation compound associated with configurational $s^{conf}(x,T)$, vibrational $s^{vib}(x,T)$, and electronic $s^{elec}(x,T)$ excitations. These expressions are then used to shed light on the behavior of the entropic potential $\partial U_{ocv}(x,T)/\partial T$ of the battery.

2.2.2. Configurational Entropy, $s^{conf}_{Li_xMA}(x,T)$. The configurational entropy of an intercalation compound, Li_xMA, exhibiting a solid solution is bounded by the *ideal* solution configurational entropy expressed as[45]

$$s^{conf}_{Li_xMA}(x,\,T) = -k_B[x\,\ln(x) + (1-x)\,\ln(1-x)] \qquad (14)$$

The configurational entropies of stoichiometric LiMA and MA are equal to zero (i.e., $s^{conf}_{LiMA} = 0$ and $s^{conf}_{MA} = 0$) since no disorder exists among Li ions and vacancies when all Li sites are fully filled ($x = 1$) or completely empty ($x = 0$). It is also interesting to note that this contribution is independent of the material MA. Figure 3a plots $s^{conf}_{Li_xMA}(x,T)$ of Li_xMA predicted by eq 14 as a function of lithium composition x, and featuring a maximum at half-filling or $x = 0.5$.

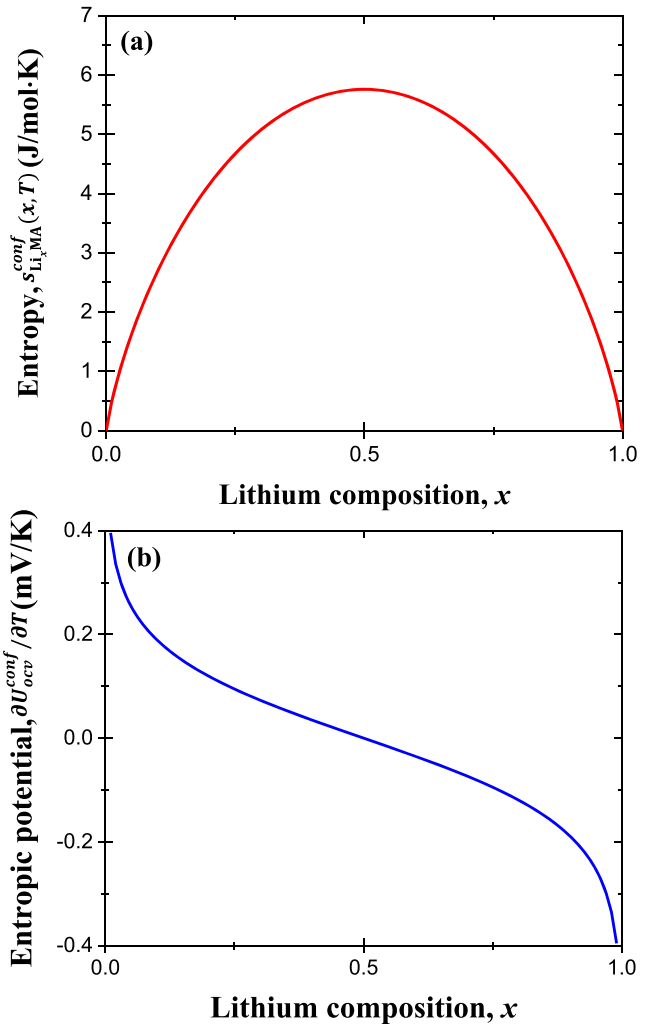

Figure 3. (a) Calculated configurational entropy $s^{conf}_{Li_xMA}(x,T)$ of Li_xMA [eq 14] and (b) configurational entropic potential $\partial U^{conf}_{ocv}(x,T)/\partial T$ of the battery cell [eq 15] as functions of lithium composition x for an *ideal* homogeneous solid solution Li_xMA.

The configurational entropy of a real intercalation compound is always smaller than the *ideal* solution entropy since interactions among Li ions lead to some degree of short-range order and therefore a lowering of the entropy. There are also instances when the Li ions and vacancies adopt a long-range ordered pattern at a specific stoichiometric composition characterized by a supercell periodicity.[46] Then, the configurational entropy for an ordered phase exhibits a minimum in the form of a cusp at the stoichiometric ordering concentration, as discussed later.

Finally, since the configurational entropy of the metallic Li anode vanishes, the contribution to the entropic potential from configurational excitations for an *ideal* solid solution simplifies to

https://doi.org/10.1021/acs.jpcc.1c10414
J. Phys. Chem. C 2022, 126, 6096−6110

$$\frac{\partial U_{ocv}^{conf}(x,\,T)}{\partial T} = \frac{1}{e}\frac{\partial s_{Li_xMA}^{conf}(x,\,T)}{\partial x} = -\frac{k_B}{e}\ln\left(\frac{x}{1-x}\right) \tag{15}$$

Figure 3b shows that the configurational entropic potential $\partial U_{ocv}^{conf}(x,T)/\partial T$ decreases monotonically for an *ideal* homogeneous solid solution Li_xMA upon lithiation.

2.2.3. Vibrational Entropy, $s^{vib}(x,T)$. In general, the vibrational entropy is a function of the lithium composition x due to the change in the number of Li ions and to changes in the nature and strength of bonds between the host ions as Li intercalates into the crystal. It can be quantified using the harmonic approximation and depends on the stiffness of interatomic bonds within the compound.[44]

The vibrational Helmholtz free energy $f_{MA}^{vib}(T)$ of the host intercalation compound MA at constant volume v can be expressed as an integral over all phonon-mode frequencies according to[47]

$$f_{MA}^{vib}(T) = k_B T\int_0^\infty \left[\frac{\hbar\omega}{2k_B T} + \ln(1 - e^{\hbar\omega/k_B T})\right]\mathcal{D}^{vib}(\omega)\,d\omega \tag{16}$$

Here, $\hbar$ is the reduced Planck constant, and $\mathcal{D}^{vib}(\omega)$ is the phonon density of states corresponding to the number of vibrational normal modes per unit cell of the intercalation compound with a frequency ω. It is determined from the phonon dispersion relationship and, in general, depends on volume. By definition, the Gibbs free energy $g_{MA}^{vib}(T)$ is the characteristic potential at constant pressure of compound MA and is related to the Helmholtz free energy $f_{MA}^{vib}(T)$ according to

$$g_{MA}^{vib}(T) = f_{MA}^{vib}(T) + Pv(T) \tag{17}$$

where $v(T)$ is the equilibrium volume per unit cell at the imposed pressure P. Then, the vibrational entropy $s_{MA}^{vib}(T)$ can be extracted from the vibrational Gibbs free energy using eq 10.

A change in the lithium composition of the intercalation compound MA can affect its vibrational free energy in two ways. First, the insertion of Li ions into MA introduces additional vibrational modes, three for each inserted Li ion. Second, a change in the lithium composition x affects the stiffness of the bonds of the host intercalation compound. For example, the redox processes on the transition metals that accompany variations in x often lead to some degree of rehybridization between the transition metals and the anions,[48,49] which in turn affects the stiffness of their bonds.

As with configurational entropy, it is useful to consider the vibrational entropy for an ideal intercalation compound. With respect to vibrational excitations, we define an *ideal* intercalation compound as one that accommodates Li without changing the vibrational spectrum and the phonon density of states $\mathcal{D}^{vib}(\omega)$ of the host MA. Furthermore, we assume that the vibrational spectrum of the Li ions can be approximated by the Einstein model with a characteristic frequency ω_{Li} independent of the overall lithium composition and volume of the host. Under these assumptions, the vibrational Gibbs free energy $g_{Li_xMA}^{vib}(x,T)$ of Li_xMA can be expressed as

$$g_{Li_xMA}^{vib}(x,\,T) = g_{MA}^{vib}(T) + g_{Li}^{vib}(x,\,T) \tag{18}$$

where $g_{MA}^{vib}(T)$ is the vibrational free energy of the host without Li [eq 17] and $g_{Li}^{vib}(x,T)$ captures the contributions to the vibrational free energy from Li vibrations in interstitial sites of the MA host. Assuming a constant characteristic vibrational frequency ω_{Li} for Li, $g_{Li}^{vib}(x,T)$ can be written as

$$g_{Li}^{vib}(x,\,T) = 3\left[\frac{\hbar\omega_{Li}}{2} + k_B T\ln(1 - e^{-\hbar\omega_{Li}/k_B T})\right]x \tag{19}$$

This expression emerges when imposing the approximations of ideality as previously defined in the evaluation of the vibrational partition function, as shown in Supporting Information. Combining eqs 10, 18, and 19 yields the expression of the vibrational entropy

$$s_{Li_xMA}^{vib}(x,\,T) = s_{MA}^{vib}(T) - 3k_B\left[\ln(1 - e^{-\Theta_{Li}/T}) - \frac{\Theta_{Li}}{T}\frac{e^{-\Theta_{Li}/T}}{1 - e^{-\Theta_{Li}/T}}\right]x \tag{20}$$

where $\Theta_{Li} = \hbar\omega_{Li}/k_B$. This expression shows that the vibrational entropy of an *ideal* intercalation compound is a linear function of the lithium composition x, as plotted in Figure 4a. Figure 4a also shows that both the magnitude and the slope of $s_{Li_xMA}^{vib}(x,T)$ decreases with increasing ω_{Li}.

The contribution from vibrational excitations to the entropic potential for an *ideal* intercalation compound can be written, using eq 11, as

$$\frac{\partial U_{ocv}^{vib}(x,\,T)}{\partial T} = -\frac{1}{e}\left[3k_B\left(\ln(1 - e^{-\Theta_{Li}/T}) - \frac{\Theta_{Li}}{T}\frac{e^{-\Theta_{Li}/T}}{1 - e^{-\Theta_{Li}/T}}\right) + s_{Li}^{o,vib}(T)\right] \tag{21}$$

where $s_{Li}^{o,vib}(T)$ is the vibrational entropy of metallic Li. Here, $s_{MA}^{vib}(T)$ disappeared upon differentiation with respect to the lithium composition x. Experimentally, the average vibrational frequency ω_{Li} of metallic Li was measured to be on the order of 10^{12} Hz from slow-neutron scattering.[50] An effective vibrational frequency for metallic Li can also be estimated when assuming that the entropy of metallic Li is dominated by the vibrational entropy. This leads to an effective frequency ω_{Li} of 5.8×10^{12} Hz.[36] Figure 4a shows that the vibrational entropy $s_{Li_xMA}^{vib}(x,T)$ of Li_xMA linearly increases with lithium composition x. Thus, the entropic potential $\partial U_{ocv}^{vib}(x,T)/\partial T$ of the battery cell is independent of x (Figure 4b). In real intercalation compounds, the insertion of Li into the host introduces a composition dependence to the host vibrational entropy $s_{MA}^{vib}(x,T)$ that does not cancel upon differentiation with respect to x. Furthermore, even when applying a simple Einsten model for the vibrational excitations of the intercalated Li ions, it is unlikely that the Li vibrational frequency ω_{Li} remains independent of x. Hence, in real intercalation compounds, the contribution from vibrational excitations to $\partial U_{ocv}^{vib}(x,T)/\partial T$ features a composition dependence. In binary systems, the variation of the vibrational entropy with composition x is generally assumed to be linear.[41,51,52] However, to the best of our knowledge, detailed studies to quantify the extent with which $s_{MA}^{vib}(T)$ differs from zero in intercalation compounds have not yet been performed. Overall, the vibrational entropy $s_{Li_xMA}^{vib}(x,T)$ of an *ideal* homogeneous solid solution was shown to increase linearly

https://doi.org/10.1021/acs.jpcc.1c10414
J. Phys. Chem. C 2022, 126, 6096−6110

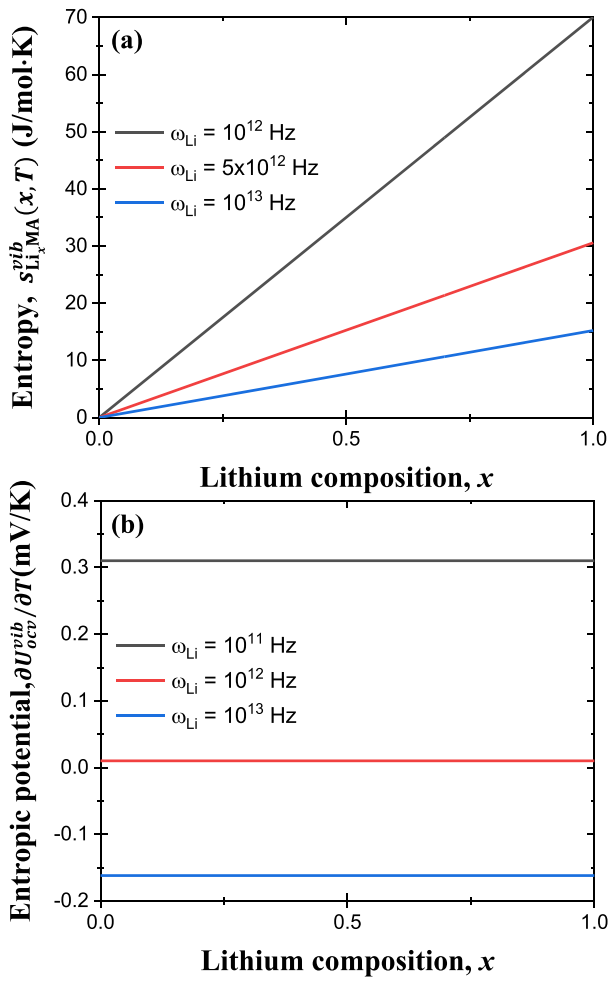

Figure 4. (a) Vibrational entropy $s^{vib}_{Li_xMA}(x,T)$ of Li_xMA [eq 20], and (b) vibrational entropic potential $\partial U^{vib}_{ocv}(x,T)/\partial T$ of the battery cell [eq 21] as functions of lithium composition x for an *ideal* solid solution Li_xMA.

with lithium composition x, leading to a vibrational entropic potential $\partial U^{vib}_{ocv}(x,T)/\partial T$ that is independent of x.

2.2.4. Electronic Entropy, $s^{elec}(x,T)$. The entropy contribution $s^{elec}(x,T)$ due to electronic excitations can have a variety of forms. The entropy of itinerant electrons is generally small and negligible.[45] However, the entropy of intercalation compounds that exhibit distinct redox states that are localized on the transition metals can be sizable and is a type of configurational entropy that emerges from the many different ways of arranging distinct oxidation states over the transition metal cations.[53] If transition metals are magnetic, an additional configurational entropy may exist in association with the many possible ways of ordering local magnetic moments over the transition metal sites.[54−56] These configurational degrees of freedom associated with localized electronic states can exhibit a lithium composition dependence.

For itinerant electrons, the electronic entropy can be expressed as[47]

$$s^{elec}(x,T) = -k_B \int [\mathcal{F}(\epsilon)\ln[\mathcal{F}(\epsilon)] + [1-\mathcal{F}(\epsilon)]\ln[1-\mathcal{F}(\epsilon)]]\mathcal{D}^{elec}(\epsilon)\,d\epsilon \quad (22)$$

where $\mathcal{F}(\epsilon)$ is the Fermi−Dirac distribution and $\mathcal{D}^{elec}(\epsilon)$ is the electronic density of states per unit cell. The electronic entropy depends on the shape of the electronic density of states $\mathcal{D}^{elec}(\epsilon)$ and the position of the Fermi level ϵ_F. The Li ions that intercalate into the compound generally donate their electrons to the host, thereby affecting the position of the Fermi level. The presence of Li and the donation of electrons to the host also modify the band structure and therefore affect the electronic density of states. Thus, Li ion intercalation introduces a composition dependence to the electronic entropy of the intercalation compound.

Based on eq 11, the electronic entropic potential $\partial U^{elec}_{ocv}(x,T)/\partial T$ can be expressed as

$$\frac{\partial U^{elec}_{ocv}(x,T)}{\partial T} = \frac{1}{e}\left[\frac{\partial s^{elec}_{Li_xMA}(x,T)}{\partial T} - s^{o,elec}_{Li}(T)\right] \quad (23)$$

where $s^{o,elec}_{Li}(T)$ is the electronic entropy of the metallic Li anode. When the density of states of body centered cubic Li is calculated from density functional theory, $s^{o,elec}_{Li}(T)$ evaluates to 0.16 J/mol·K (see the Supporting Information). In order to further investigate the shape of $\partial s^{elec}_{Li_xMA}(x,T)/\partial T$, it is again convenient to introduce the concept of ideality with respect to electronic excitations. We define an *ideal* intercalation compound as one whose electronic density of states are unaffected by the intercalation of Li. The only effect of Li insertion is to raise the Fermi level ϵ_f. This is equivalent to assuming a rigid band model.[57] While this assumption of ideality simplifies the analysis considerably, some degrees of freedom still remain with respect to the shape of the electronic density of states.

The electronic density of states $\mathcal{D}^{elec}_{Li_xMA}(\epsilon)$ could be constant as a function of the electronic energy ϵ. In this scenario, the electronic entropy $s^{elec}_{Li_xMA}(x,T)$ of Li_xMA and the electronic entropic potential $\partial U^{elec}_{ocv}(x,T)/\partial T$ would be independent of the lithium composition x (see the Supporting Information). Other simple shapes for $\mathcal{D}^{elec}(\epsilon)$ are also possible such as a box shape and a square-root dependence on ϵ, as schematically illustrated in parts a and b of Figure 5, respectively. The composition dependence of the electronic entropy $s^{elec}_{Li_xMA}(x,T)$ for these density of states curves are shown in parts c and d of Figure 5. Note that for a box-shaped density of states, the area under the differently proportioned boxes are all equal to one electron per unit cell of host material. Figure 5c shows that the magnitude of the electronic entropy for the differently proportioned box-shaped $\mathcal{D}^{elec}(\epsilon)$ increases when the width of the boxes become narrower. Likewise, the magnitude of the electronic entropy for $\mathcal{D}^{elec}(\epsilon)$ with a square-root dependence on ϵ having different constant prefactors increases with increasing magnitude of $\mathcal{D}^{elec}(\epsilon)$ (Figure 5d). These results show that the electronic entropy is sensitive to the shape of the electronic density of states. parts e and f of Figure 5 show the electronic entropic potential $\partial U^{elec}_{ocv}(x,T)/\partial T$ corresponding to box-shaped and square-root-shaped density of states, respectively. In both cases, the magnitude of $\partial U^{elec}_{ocv}(x,T)/\partial T$ is negligible compared to that of the vibrational and configurational entropic potentials modeled in the previous sections.

2.2.5. Summary. For an *ideal* intercalation compound, the entropy can be expressed as the sum of individual contributions derived in previous subsections (eq 13). Figure

https://doi.org/10.1021/acs.jpcc.1c10414
J. Phys. Chem. C 2022, 126, 6096−6110

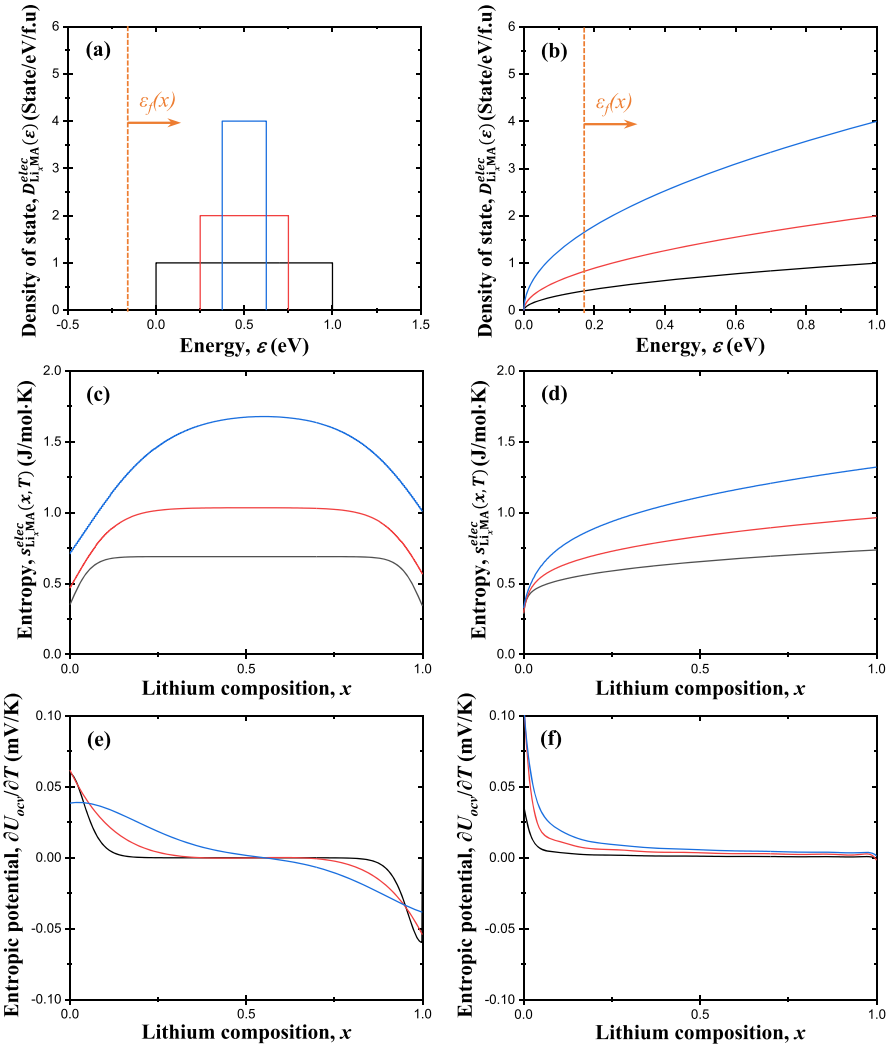

Figure 5. (a) Box-shaped and (b) square-root-shaped density of state $\mathcal{D}^{\text{elec}}_{\text{Li}_x\text{MA}}(\epsilon)$ of Li_xMA as functions of electric energy ϵ. Electronic entropy $s^{elec}_{\text{Li}_x\text{MA}}(x,T)$ of Li_xMA corresponding to (c) a box-shaped $\mathcal{D}^{\text{elec}}_{\text{Li}_x\text{MA}}(\epsilon)$ and (d) a square-root-shaped $\mathcal{D}^{\text{elec}}_{\text{Li}_x\text{MA}}(\epsilon)$ and electronic entropic potential $\partial U^{elec}_{ocv}(x,T)/\partial T$ of a battery cell for (e) a box-shaped $\mathcal{D}^{\text{elec}}_{\text{Li}_x\text{MA}}(\epsilon)$ and (f) a square-root-shaped $\mathcal{D}^{\text{elec}}_{\text{Li}_x\text{MA}}(\epsilon)$ as functions of lithium composition x.

6a shows the calculated entropy associated with configurational $s^{conf}_{\text{Li}_x\text{MA}}(x,T)$, vibrational $s^{vib}_{\text{Li}_x\text{MA}}(x,T)$, and electronic $s^{elec}_{\text{Li}_x\text{MA}}(x,T)$ excitations predicted respectively by eqs 14, 20, and 22, as well as the entropy of the Li_xMA electrode, i.e., $s_{\text{Li}_x\text{MA}}(x,T) = s^{conf}_{\text{Li}_x\text{MA}}(x,T)+s^{vib}_{\text{Li}_x\text{MA}}(x,T)+s^{elec}_{\text{Li}_x\text{MA}}(x,T)$. Here, the vibrational frequency ω_{Li} was taken as 10^{13} Hz. The Einstein model and the square−root−shaped electronic density of state $\mathcal{D}^{\text{elec}}(\epsilon)$ were used to estimate $s^{vib}_{\text{Li}_x\text{MA}}(x,T)$, and $s^{elec}_{\text{Li}_x\text{MA}}(x,T)$, respectively. Figure 6a illustrates that $s^{elec}_{\text{Li}_x\text{MA}}(x,T)$ is relatively small compared to $s^{conf}_{\text{Li}_x\text{MA}}(x,T)$ and $s^{vib}_{\text{Li}_x\text{MA}}(x,T)$. Furthermore, the trend of $s_{\text{Li}_x\text{MA}}(x,T)$ is mostly governed by $s^{vib}(x,T)$ so that it increases with increasing lithium composition x.

Moreover, Figure 6b shows the calculated entropic potential associated with configurational $\partial U^{conf}_{ocv}(x,T)/\partial T$, vibrational $\partial U^{vib}_{ocv}(x,T)/\partial T$, and electronic $\partial U^{elec}_{ocv}(x,T)/\partial T$ excitations predicted respectively by eqs 15, 21, and 23 as well as the battery entropic potential $\partial U_{ocv}(x,T)/\partial T$. Here, $\partial U^{vib}_{ocv}(x,T)/\partial T$ is independent of lithium composition x and is negative due to the Li metal counter electrode. Likewise, $\partial U^{elec}_{ocv}(x,T)/\partial T$ is approximately constant and its magnitude is negligible compared to that of $\partial U^{conf}_{ocv}(x,T)/\partial T$ and $\partial U^{vib}_{ocv}(x,T)/\partial T$. The trend of the $\partial U_{ocv}(x,T)/\partial T$ curve is dominated by $\partial U^{conf}_{ocv}(x,T)/\partial T$. Overall, an *ideal* intercalation compound forming a homogeneous solid solution is characterized by monotonically decreasing $\partial U_{ocv}(x,T)/\partial T$ with increasing lithium composition x.

2.3. Ion Ordering from a Homogeneous Solid Solution. It is common for the guest cations of an intercalation compound to order at specific stoichiometric compositions. For example, the Li ions and vacancies of layered Li_xCoO_2 adopt an ordered arrangement at $x = 0.5$[12,48] while the Na ions of Na_xCoO_2 form a devil's staircase of orderings over a range of compositions.[58] Guest cation ordering generally leads to spontaneous symmetry breaking and the emergence of a superlattice with some sublattices preferentially occupied by the guest cation and the others remaining vacant.[46] For most ordering reactions, the symmetry breaking can be detected with diffraction.[12] In this section, we

https://doi.org/10.1021/acs.jpcc.1c10414
J. Phys. Chem. C 2022, 126, 6096−6110

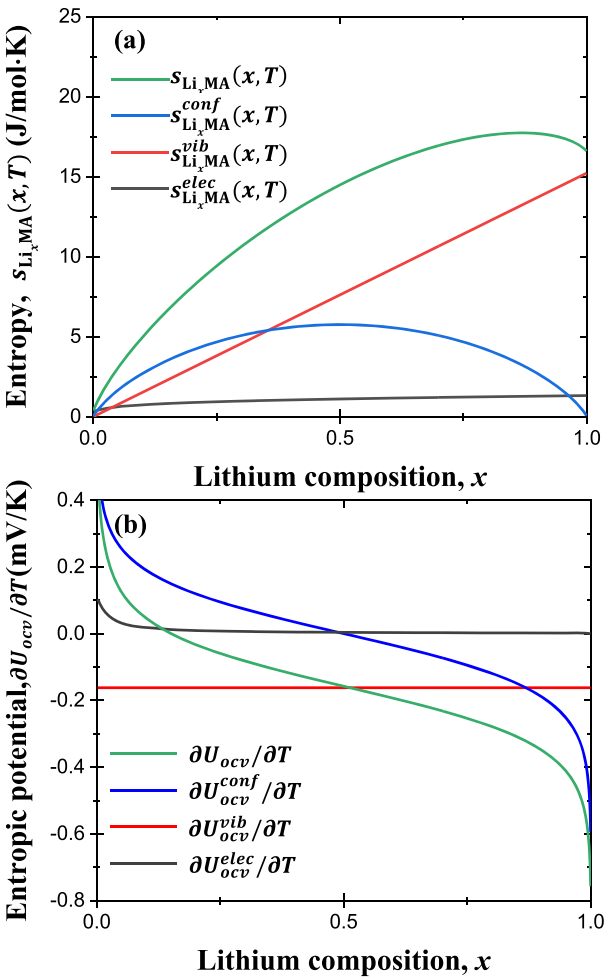

Figure 6. (a) Calculated entropy associated with configurational $s^{conf}_{Li_xMA}(x,T)$, vibrational $s^{vib}_{Li_xMA}(x,T)$, and electronic $s^{elec}_{Li_xMA}(x,T)$ excitations as well as the entropy of the Li_xMA electrode, i.e., $s_{Li_xMA}(x,T) = s^{conf}_{Li_xMA}(x,T)+s^{vib}_{Li_xMA}(x,T)+s^{elec}_{Li_xMA}(x,T)$. (b) Calculated entropic potential associated with configurational $\partial U^{conf}_{ocv}(x,T)/\partial T$, vibrational $\partial U^{vib}_{ocv}(x,T)/\partial T$, and electronic $\partial U^{elec}_{ocv}(x,T)/\partial T$ excitations as well as the entropic potential of the battery, i.e., $\partial U_{ocv}(x,T)/\partial T = \partial U^{conf}_{ocv}(x,T)/\partial T + \partial U^{vib}_{ocv}(x,T)/\partial T + \partial U^{elec}_{ocv}(x,T)/\partial T$.

explore how an ordering reaction manifests itself in the entropic potential $\partial U_{ocv}(x,T)/\partial T$.

While the emergence of an ordered phase arises from interactions among the guest cations, the entropy of an ordering reaction can also be explored with a simplified model that neglects such interactions. By introducing sublattices with different guest ion site energies, it is possible to extend the ideal solution model to one that exhibits features of common ordering reactions. The intercalated Li will then selectively fill the more favorable sublattice sites first, before filling the less favorable sites. We consider a model where interactions between Li ions are neglected, but where half the sites form a sublattice that hosts Li at a lower energy (sublattice 2) than the other half of available sites (sublattice 1). It is convenient to introduce sublattice concentrations x_1 and x_2 tracking the fraction of occupied sites on sublattice 1 and 2, respectively.[42,46] The overall Li concentration is related to the sublattice concentrations according to $x = (x_1 + x_2)/2$ when the number of sites on the two sublattices are equal.

The free energy of an ideal intercalation compound with two sublattices can be expressed as

$$g_{Li_xMA}(x, T) = g_{MA}(T) + \epsilon_1 x_1 + \epsilon_2 x_2 + k_B T[x_1 \ln(x_1) + (1 - x_1)\ln(1 - x_1)] + k_B T[x_2 \ln(x_2) + (1 - x_2)\ln(1 - x_2)] \quad (24)$$

where ϵ_1 and ϵ_2 are sublattice site energies such that $\epsilon_1 \geq \epsilon_2$. These energies may be temperature-dependent if vibrational excitations are accounted for. The ideal solution entropy measures the configurational entropy of noninteracting Li ions on each sublattice. The free energy model has one independent variable at fixed Li concentration x. Since Li can freely distribute between the two sublattices, one of the sublattice concentrations, e.g., x_1, is an independent variable while x_2 is a dependent variable such that $x_2 = 2x - x_1$. Under thermodynamic equilibrium, x_1 adopts the value that minimizes the free energy (eq 24). It is the equilibrium value of x_1 that must be inserted into eq 24 to obtain the equilibrium free energy and all its derived properties, including the Li chemical potential and the entropy (see the Supporting Information). The thermodynamic properties of this model are sensitive to the relative values of ϵ_1 and ϵ_2. The parameter $\theta = \epsilon_1/\epsilon_2$ can be used to model different scenarios. Figure 7a shows the lowest Gibbs free energy $g_{Li_xMA}(x,T)$ as only a function of x for different values of $\theta = \epsilon_1/\epsilon_2$. When $\theta = 1$, we recover the *ideal* solution model without any sublattice site preference. Then, the minimum free energy as a function of x occurs for $x_1 = x_2 = x$ such that the equilibrium free energy of eq 24 reduces to that of an ideal solution. A value of $\theta = \epsilon_1/\epsilon_2 > 1$ leads to a Li preference for sublattice 2 when ϵ_1 and ϵ_2 are both positive. Increasing θ leads to an increased degree of segregation to the more favorable sublattice and to a step in the open circuit voltage $U_{ocv}(x,T)$ at $x = 0.5$, as illustrated in Figure 7b. The step occurs when the more favorable site becomes fully saturated and additional Li ions are required to fill energetically less favorable sites. The resulting ordering around $x = 0.5$ leads to a dip in the entropy $s_{Li_xMA}(x,T)$, as evident in Figure 7c. Figure 7d shows that the battery entropic potential $\partial U_{ocv}(x,T)/\partial T$ exhibits an inflection point at $x = 0.5$ in the models that undergo a strong ordering reaction.

Although we have considered an idealized model to elucidate the effect of ion ordering on the entropy and the entropic potential, similar features are evident in real intercalation compounds that undergo order/disorder reactions. Both Li_xTiS_2 and Li_xCoO_2 are examples of intercalation compounds that exhibit ordered phases. Layered Li_xTiS_2 forms a solid solution for most values of x but undergoes a staging reaction around $x \approx 0.2$, whereby Li segregates to every other Li layer.[9,59] Figure 8a shows experimental measurements of $U_{ocv}(x,T)$ and $\partial U_{ocv}(x,T)/\partial T$ for a battery system with a TiS_2 working electrode and a lithium metal counter electrode during lithiation. The electrolyte consisted of a mixture of 1 M of $LiPF_6$ with ethylene carbonate (EC) and dimethyl carbonate (DMC). The trend of the measured $U_{ocv}(x,T)$ and $\partial U_{ocv}(x,T)/\partial T$ were in a good agreement with the literature.[9] The open circuit voltage $U_{ocv}(x,T)$ exhibited the characteristic shape of a solid solution above $x \approx 0.4$. While a pronounced step at $x \approx 0.2$ was not directly evident in $U_{ocv}(x,T)$, the entropic potential $\partial U_{ocv}(x,T)/\partial T$ featured a fluctuation in the form of a tilde due

https://doi.org/10.1021/acs.jpcc.1c10414
J. Phys. Chem. C 2022, 126, 6096−6110

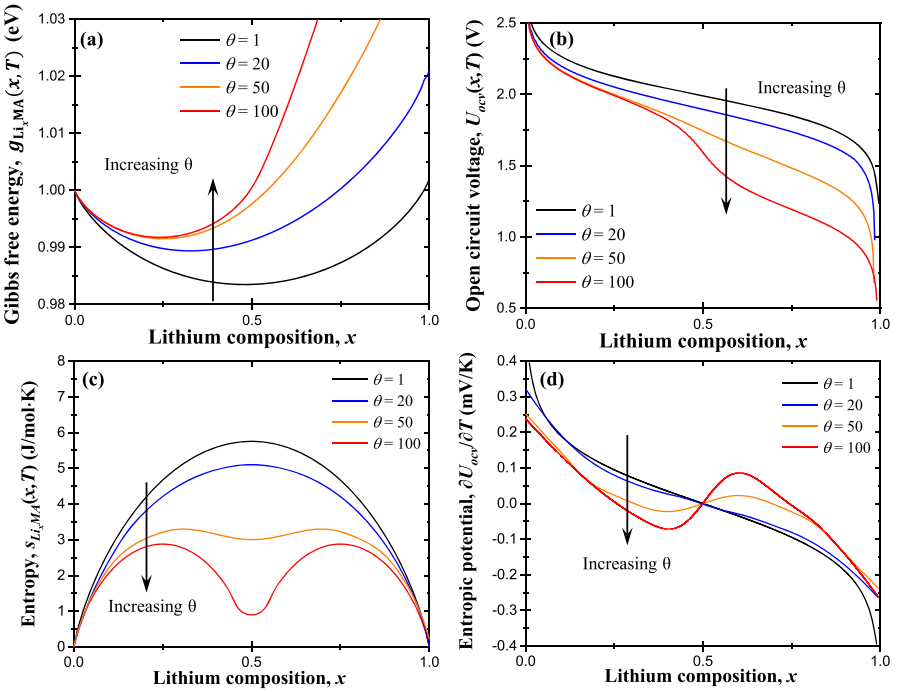

Figure 7. (a) The Gibbs free energy $g_{Li_xMA}(x,T)$ of Li_xMA, (b) the open circuit voltage $U_{ocv}(x,T)$ of the battery cell, (c) the entropy $s_{Li_xMA}(x,T)$ of Li_xMA, and (d) the entropic potential $\partial U_{ocv}(x,T)/\partial T$ of the battery cell as functions of lithium composition x at temperature T with varying $\theta = \epsilon_1/\epsilon_2$.

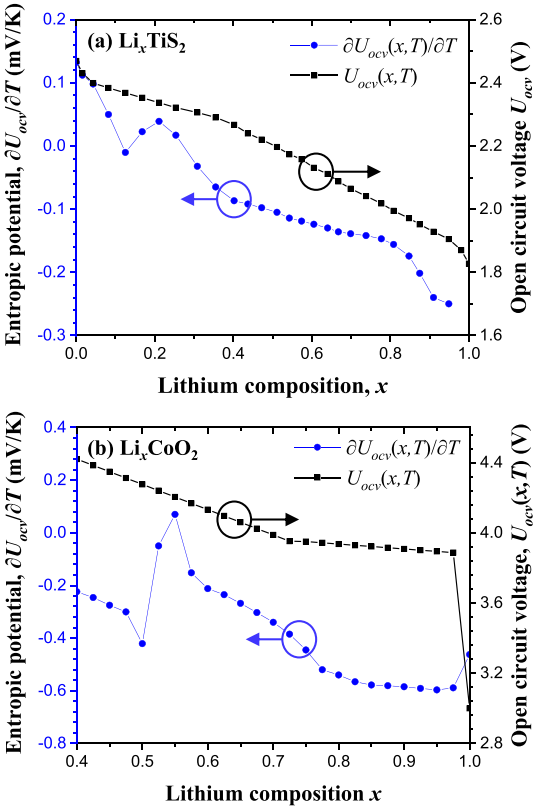

Figure 8. Measured open circuit voltage $U_{ocv}(x,T)$ and entropic potential $\partial U_{ocv}(x,T)/\partial T$ as functions of lithium composition x in (a) Li_xTiS_2 during lithiation and (b) Li_xCoO_2 during delithiation.

to the occurrence of stage ordering analogous to that of Figure 7d for the ideal model.

Li_xCoO_2 is another intercalation compound that exhibits an ordered phase.[12,48] Here, the Li ions of Li_xCoO_2 can occupy octahedrally coordinated interstitial sites that form two-dimensional triangular lattices. At x = 0.5 the Li ions adopt an ordered arrangement in which they line up into rows separated by rows of vacancies within each layer.[12] Figure 8b shows $U_{ocv}(x,T)$ and $\partial U_{ocv}(x,T)/\partial T$ measured for a battery system consisting of a $LiCoO_2$ working electrode and a lithium metal counter electrode with 1 M of $LiPF_6$ in an EC/DMC mixture as electrolyte during delithiation. Here also, $\partial U_{ocv}(x,T)/\partial T$ featured a tilde-shaped fluctuation similar to that observed in the TiS_2 electrode (Figure 8a) due to the intralayer ion ordering in the range of $0.45 \leq x \leq 0.55$.[45,60] Even though the trends of both $U_{ocv}(x,T)$ and $\partial U_{ocv}(x,T)/\partial T$ were in a good agreement with those reported in previous studies,[28,45,61] the magnitude of $\partial U_{ocv}(x,T)/\partial T$ in the ion ordering region ($0.45 \leq x \leq 0.55$) varied among studies.[28,45,61] This effect can possibly be due to the different C-rates used since intralayer ion ordering is sensitive to the kinetics of ions transport within the active electrode material.[28] In addition to an ordering reaction, Li_xCoO_2 also underwent a first-order phase transformation from a metallic solid solution at x = 0.75 to a semiconducting solid solution at x = 0.93, as confirmed with *in situ* XRD measurements.[12] This was also evident in both the $\partial U_{ocv}(x,T)/\partial T$ and $U_{ocv}(x,T)$ curves, which were almost constant for $0.75 > x > 0.93$. The next section analyzes the behavior of $\partial U_{ocv}(x,T)/\partial T$ during a first-order phase transformation.

2.4. Phase Transition Accompanied by a Two-Phase Coexistence Region. An intercalation compound MA may undergo a first-order phase transition, as observed at the high lithium compositions in Li_xCoO_2, from a lithium-poor α-phase

https://doi.org/10.1021/acs.jpcc.1c10414
J. Phys. Chem. C 2022, 126, 6096−6110

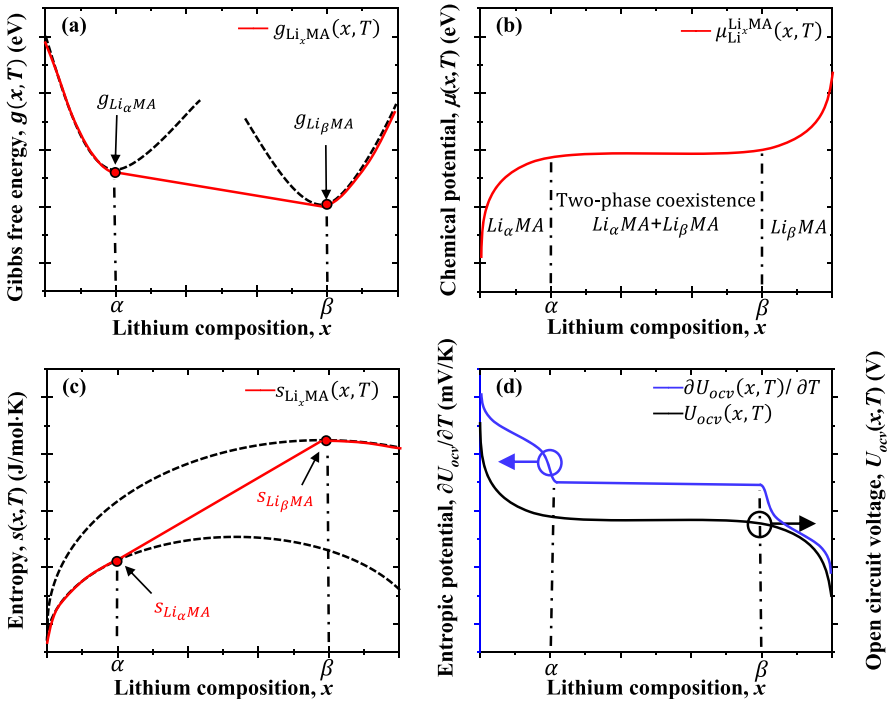

Figure 9. (a) Schematic plots of Gibbs free energy $g_{Li_xMA}(x,T)$, (b) chemical potential $\mu_{Li}^{Li_xMA}(x,T)$, (c) entropy $s_{Li_xMA}(x,T)$ of Li_xMA, and (d) Open circuit voltage $U_{ocv}(x,T)$ and entropic potential $\partial U_{ocv}(x,T)/\partial T$ of the battery cell as functions of lithium composition x at temperature T during a first order phase transition accompanied by a lithium poor phase $Li_\alpha MA$ coexisting with a lithium-rich phase $Li_\beta MA$.

to a lithium-rich β-phase upon the insertion of Li. During such a phase transition, both the α- and β-phases coexist. Figure 9a schematically shows the Gibbs free energies $g_{Li_\alpha MA}(T)$ and $g_{Li_\beta MA}(T)$ of coexisting phases. The common tangent construction determines the equilibrium concentrations of the two coexisting phases. The free energy of the two-phase mixture resides on the common tangent between the lithium poor phase $Li_\alpha MA$ with composition α and the lithium rich phase $Li_\beta MA$ with composition β. Thus, the Gibbs free energy $g_{Li_xMA}(\alpha \le x \le \beta, T)$ in the two-phase coexistence region can be written as

$$g_{Li_xMA}(\alpha \le x \le \beta, T) = g_{Li_\alpha MA}(T) + \frac{g_{Li_\beta MA}(T) - g_{Li_\alpha MA}(T)}{\beta - \alpha}(x - \alpha) \quad (25)$$

The Li chemical potential $\mu_{Li}^{Li_xMA}(\alpha \le x \le \beta, T)$ of the host material Li_xMA in the two-phase coexistence region is then given by

$$\mu_{Li}^{Li_xMA}(\alpha \le x \le \beta, T) = \frac{\partial g_{Li_xMA}(\alpha \le x \le \beta, T)}{\partial x} = \frac{g_{Li_\beta MA}(T) - g_{Li_\alpha MA}(T)}{\beta - \alpha} \quad (26)$$

Thus, $\mu_{Li}^{Li_xMA}(\alpha \le x \le \beta, T)$ remains constant in the two-phase coexistence region, as illustrated in Figure 9b.

Figure 9c shows the entropy $s_{Li_xMA}(x,T)$ of the host material as a function of lithium composition x. The coexisting α- and β-phases are treated as solid solutions such that their entropies exhibit the characteristic dome-shaped curves of a solid solution. Here, the entropy of the α-phase was arbitrarily chosen to be smaller than that of the β-phase. Here also, the entropy of the two-phase mixture resides on the chord connecting $s_{Li_\alpha MA}$ and $s_{Li_\beta MA}$.

The open circuit voltage $U_{ocv}(\alpha \le x \le \beta, T)$ in the two-phase coexistence region can be expressed as

$$U_{ocv}(\alpha \le x \le \beta, T) = -\frac{1}{e}\left[\frac{g_{Li_\beta MA}(T) - g_{Li_\alpha MA}(T)}{\beta - \alpha} - g_{Li}^{o}(T)\right] \quad (27)$$

Thus, the corresponding entropic potential in the two-phase coexistence region is given by

$$\frac{\partial U_{ocv}}{\partial T}(\alpha \le x \le \beta, T) = \frac{1}{e}\left[\frac{s_{Li_\beta MA}(T) - s_{Li_\alpha MA}(T)}{\beta - \alpha} - s_{Li}^{o}(T)\right] \quad (28)$$

Overall, these results indicate that both $U_{ocv}(x,T)$ and $\partial U_{ocv}(x,T)/\partial T$ are constant and independent of x in the two-phase coexistence region, as illustrated in Figure 9d.

To illustrate the predicted behavior of $U_{ocv}(x,T)$ and $\partial U_{ocv}(x,T)/\partial T$ given by eqs 27 and 28 in a two-phase coexistence region, Figure 10a shows experimental measurements for a battery system consisting of a $Li_{4/3}Ti_{5/3}O_4$ working electrode and a lithium metal counter electrode with 1.2 M of $LiPF_6$ in an EC/DMC electrolyte as a function of the lithium composition x during lithiation.[37] EELS and *in situ* XRD measurements indicated a first order phase transition from spinel $Li_{4/3}Ti_{5/3}O_4$ to rock salt $Li_{7/3}Ti_{5/3}O_4$ during lithiation.[19,37,62] In fact, Figure 10a shows that both $U_{ocv}(x,T)$ and $\partial U_{ocv}(x,T)/\partial T$ were constant for $\alpha = 4/3 \le x \le 7/3 = \beta$, indicating the coexistence of the two phases $Li_{4/3}Ti_{5/3}O_4$ and $Li_{7/3}Ti_{5/3}O_4$.

https://doi.org/10.1021/acs.jpcc.1c10414
J. Phys. Chem. C 2022, 126, 6096−6110

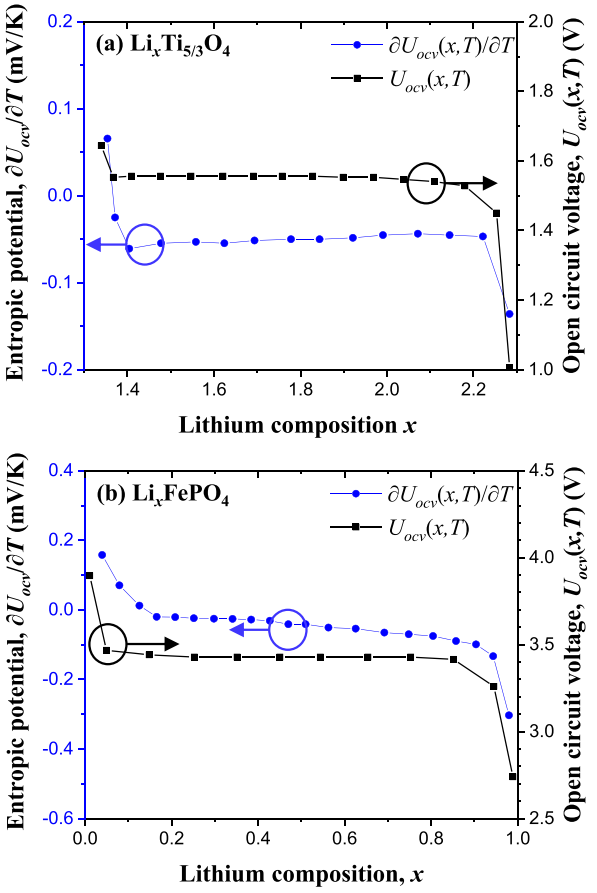

Figure 10. Open circuit voltage $U_{ocv}(x,T)$, and entropic potential $\partial U_{ocv}(x,T)/\partial T$ as functions of lithium composition x in (a) $Li_xTi_{5/3}O_4$ (data retrieved from Figure 2 in ref 37), and (b) Li_xFePO_4 (data retrieved from Figure 6 in ref 10) during lithiation.

Similarly, Figure 10b shows $U_{ocv}(x,T)$ and $\partial U_{ocv}(x,T)/\partial T$ for a battery system consisting of a $FePO_4$ working electrode and a lithium metal counter electrode in 1 M $LiPF_6$ in an EC/DMC electrolyte during lithiation.[10] Here also, electron energy-loss spectroscopy and *in situ* XRD measurements indicated a first order phase transition from $FePO_4$ to olivine $LiFePO_4$ during lithiation.[63−65] Figure 9b shows that both $U_{ocv}(x,T)$ and $\partial U_{ocv}(x,T)/\partial T$ were constant for $0 \le x \le 1$. This observation was consistent with eqs 27 and 28 for the coexistence of $FePO_4$ and $LiFePO_4$ phases. In summary, a first-order phase transition accompanied by two-phase coexistence is characterized by constant $U_{ocv}(x,T)$ and $\partial U_{ocv}(x,T)/\partial T$, as illustrated experimentally for $Li_{4/3}Ti_{5/3}O_4$ and $LiFePO_4$.

2.5. Two-Phase Coexistence with a Stable Intermediate Phase. Some intercalation compounds, such as graphite, pass through a stable intermediate phase by means of first-order phase transitions upon Li insertion. Figure 11a shows schematic Gibbs free energy curves for an intercalation compound MA that has a stable intermediate γ-phase with a composition between that of the dilute α-phase and the lithiated β-phase. The stability of the intermediate γ-phase leads to two two-phase regions as shown in Figure 11a by the common tangents between α- and γ- and between γ- and β-phases. The two common tangents result in two plateaus separated by a step in the Li chemical potential curve as schematically shown in Figure 11b.

Figure 11c schematically shows the entropy as a function of Li concentration for the different phases that can form upon Li insertion into MA. Two distinct scenarios are possible based on the value of the entropy of the intermediate γ-phase relative to that of the α- and β-phases. In Case I, $s_{Li_\gamma MA}$ lies above the chord connecting $s_{Li_\alpha MA}$ and $s_{Li_\beta MA}$, as illustrated in Figure 11c. This scenario can be expected when the intermediate phase is a solid solution, which generally exhibits its highest configurational entropy at intermediate concentrations. In Case II, the entropy $s_{Li_\gamma MA}$ of the intermediate γ-phase falls below the chord connecting $s_{Li_\alpha MA}$ and $s_{Li_\beta MA}$. This is more likely to occur if the intermediate phase corresponds to an ordered phase exhibiting a minimum at the stoichiometric ordering concentration. Figure 11d shows the associated open circuit voltage $U_{ocv}(x,T)$ and the entropic potential $\partial U_{ocv}(x,T)/\partial T$ as functions of the lithium composition x. In both cases, $U_{ocv}(x,T)$ and $\partial U_{ocv}(x,T)/\partial T$ feature two plateaus for $\alpha \le x \le \gamma$ and $\gamma \le x \le \beta$ and a step around $x = \gamma$, as observed previously for $\mu_{Li}^{Li_xMA}(x,T)$ (Figure 11b). However, in Case I, $\partial U_{ocv}(x,T)/\partial T$ is larger in the coexistence region of $Li_\alpha MA$ and $Li_\gamma MA$ ($\alpha \le x \le \gamma$) than in the coexistence region of $Li_\beta MA$ and $Li_\gamma MA$ ($\gamma \le x \le \beta$). By contrast, in Case II, $\partial U_{ocv}(x,T)/\partial T$ is smaller for $\alpha \le x \le \gamma$ than for $\gamma \le x \le \beta$.

Figure 12 shows $U_{ocv}(x,T)$ and $\partial U_{ocv}(x,T)/\partial T$ measured for a battery system consisting of a graphite working electrode and a lithium metal counter electrode in 1 M of $LiPF_6$ in an EC/DMC during lithiation. Three regions can be identified from the measured $U_{ocv}(x,T)$ and $\partial U_{ocv}(x,T)/\partial T$: (I) a homogeneous solid solution in the range of $0 \le x \le 0.25$ with monotonically decreasing $U_{ocv}(x,T)$ and $\partial U_{ocv}(x,T)/\partial T$, (II) a two-phase coexistence of LiC_{24} and LiC_{12} in the composition range $0.25 \le x \le 0.5$ with constant $U_{ocv}(x,T)$ and $\partial U_{ocv}(x,T)/\partial T$, and (III) a two-phase coexistence of LiC_{12} and LiC_6 in the range of $0.5 \le x \le 0.8$ with constant $U_{ocv}(x,T)$ and $\partial U_{ocv}(x,T)/\partial T$. These three regions were also identified with *in situ* XRD measurements and density functional theory (DFT).[66−68] The latter also identified multiple stable phases in the lithium intercalation diagram of graphite in region I ($x \le 0.25$) but some of these phases have not been observed experimentally possibly due to the formation of solid electrolyte interphase (SEI) upon cycling below 1 V vs Li/Li^+.[68,69] Furthermore, both measured $U_{ocv}(x,T)$ and $\partial U_{ocv}(x,T)/\partial T$ in region II and III were in good agreement with previous experimental studies while some deviations were evident in region I.[61,69,70] This difference can be attributed to not only the formation of SEI layer but also to different structural disorders in the carbon materials.[70] The magnitude of $\partial U_{ocv}(x,T)/\partial T$ showed sharper features for well-graphitized carbon compared with disordered carbon structure.[70] The entropic potential measurements for graphite are consistent with Case II described above. The result indicates that the intermediate LiC_{12} phase has an entropy that falls below the chord that connects the entropies of LiC_{24} and LiC_6.

3. CONCLUSION

This study reviewed and clarified the fundamental thermodynamic relationships and properties of lithium-ion battery systems having intercalation compounds as their electrochemically active cathode material. Expressions for the open circuit voltage $U_{ocv}(x,T)$ and entropic potential $\partial U_{ocv}(x,T)/\partial T$ of LIB cells were rigorously derived for *ideal* intercalation compounds.

https://doi.org/10.1021/acs.jpcc.1c10414
J. Phys. Chem. C 2022, 126, 6096−6110

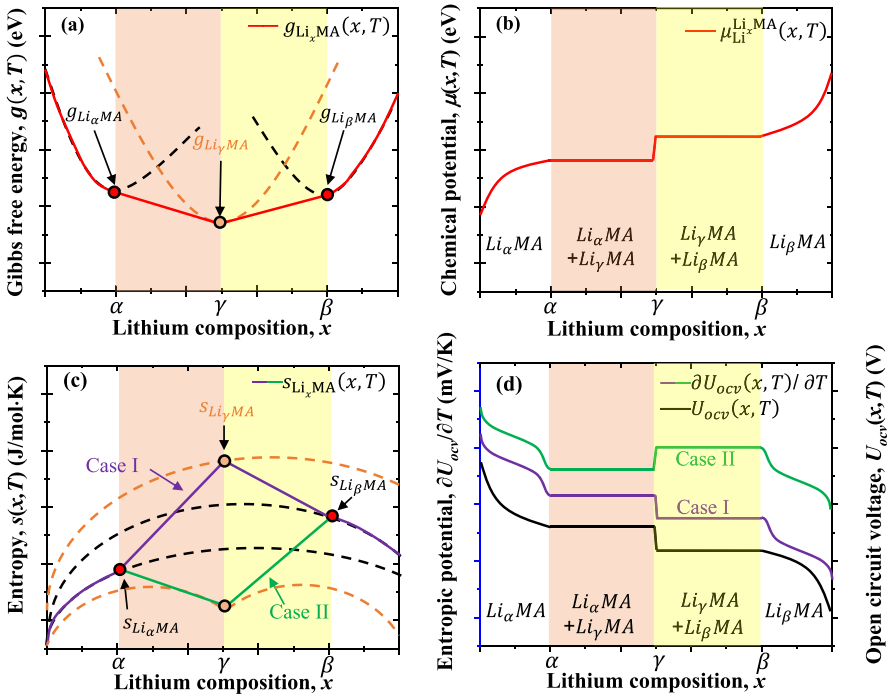

Figure 11. (a) Schematic plots of Gibbs free energy $g_{Li_xMA}(x,T)$, (b) chemical potential $\mu_{Li}^{Li_xMA}(x,T)$, (c) entropy $s_{Li_xMA}(x,T)$ of the Li_xMA, and (d) open circuit voltage $U_{ocv}(x,T)$ and entropic potential $\partial U_{ocv}(x,T)/\partial T$ of the battery cell as functions of lithium composition x at temperature T for two coexisting phases $Li_\alpha MA$ and $Li_\beta MA$ with a stable intermediate phase $Li_\gamma MA$.

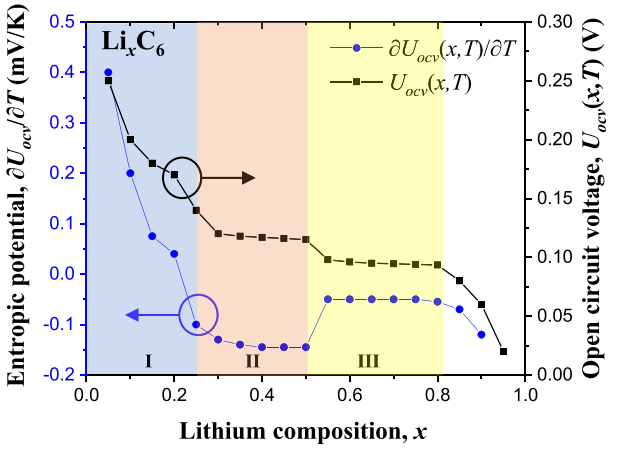

Figure 12. Open circuit voltage $U_{ocv}(x,T)$, and entropic potential $\partial U_{ocv}(x,T)/\partial T$ as functions of lithium composition x in Li_xC_6 during lithiation.

They were used to develop an interpretative guide to potentiometric entropy measurements of $U_{ocv}(x,T)$ and $\partial U_{ocv}(x,T)/\partial T$ as functions of lithium composition x for different charging/discharging mechanisms. For an ideal homogeneous solid solution, contributions from configurational, vibrational, and electronic excitations to the entropy of an ideal intercalation compound were numerically calculated to estimate the first-order behavior of $\partial U_{ocv}(x,T)/\partial T$ of a battery consisting of an intercalation compound as its cathode. The analysis suggests that general trends of $\partial U_{ocv}(x,T)/\partial T$ of a homogeneous solid solution are dominated by configurational entropy, which leads to a monotonically decreasing $U_{ocv}(x,T)$ and $\partial U_{ocv}(x,T)/\partial T$ with increasing lithium composition x. An ion ordering reaction over a subset of energetically favorable interstitial sites is characterized by a tilde-shaped fluctuation in $\partial U_{ocv}(x,T)/\partial T$ versus x. Furthermore, a first order phase transition accompanied by two-phase coexistence manifests itself as a constant $U_{ocv}(x,T)$ and $\partial U_{ocv}(x,T)/\partial T$. Finally, a two-phase coexistence with a stable intermediate phase leads to a monotonically decreasing $U_{ocv}(x,T)$ curve upon lithiation that is characterized by two plateaus separated by a step. The $\partial U_{ocv}(x,T)/\partial T$ curve for this scenario also exhibits two plateaus. However, depending on the entropy of the intermediate phase, the second plateau can either be higher or lower than the first plateau. These interpretations were systematically illustrated using experimental data for various cathode materials. The present interpretative guide can enhance other structural analysis techniques and can prove valuable in the characterization of new battery materials.

■ ASSOCIATED CONTENT

Supporting Information

The Supporting Information is available free of charge at https://pubs.acs.org/doi/10.1021/acs.jpcc.1c10414.

Experimental procedure, derivation of vibrational entropy, density functional theory calculation for lithium metal counter electrode, electronic entropy of constant electronic density of state, and free energy calculation for ion ordering from a homogeneous solid solution (PDF)

■ AUTHOR INFORMATION

Corresponding Authors

Anton Van der Ven − *Materials Department, University of California, Santa Barbara, Santa Barbara, California 93106, United States*; Phone: +1 (805)-893-7920; Email: avdv@engineering.ucsb.edu

https://doi.org/10.1021/acs.jpcc.1c10414
J. Phys. Chem. C 2022, 126, 6096−6110

Laurent Pilon − *Mechanical and Aerospace Engineering Department, Henry Samueli School of Engineering and Applied Science, California NanoSystems Institute, and Institute of the Environment and Sustainability, University of California, Los Angeles, Los Angeles, California 90095, United States;* orcid.org/0000-0001-9459-8207; Phone: +1 (310)-206-5598; Email: pilon@seas.ucla.edu; Fax: +1 (310)-206-2302

Authors

Sun Woong Baek − *Mechanical and Aerospace Engineering Department, Henry Samueli School of Engineering and Applied Science, University of California, Los Angeles, Los Angeles, California 90095, United States*

Muna Saber − *Department of Chemical Engineering, University of California, Santa Barbara, Santa Barbara, California 93106, United States*

Complete contact information is available at: https://pubs.acs.org/10.1021/acs.jpcc.1c10414

Notes

The authors declare no competing financial interest.

Biographies

Sun Woong Baek is a Ph.D. student in mechanical and aerospace engineering department at the University of California, Los Angeles (UCLA), and works under the supervision of Dr. Laurent Pilon. His research focus is on heat generation and thermodynamics of lithium-ion battery. As part of the Synthetic Control Across Length-scales for Advancing Rechargeables (SCALAR) Energy Frontier Research Center (EFRC), he is developing entropic and calorimetric measurements to gain insight into the origins of the fast-charging abilities of a variety of electrode materials.

Muna Saber is a Ph.D. student in Chemical Engineering at the University of California, Santa Barbara (UCSB), and works under the advisement of Dr. Anton Van der Ven and Dr. M. Scott Shell. Her research focus is on understanding lithiation mechanisms in fast-charging lithium-ion battery anodes using first-principles methods. Through collaboration within the Synthetic Control Across Length-scales for Advancing Rechargeables (SCALAR) EFRC, she identified the relationship between chemical strain, electronic structure, and thermodynamically stable lithium-vacancy orderings in PNb_9O_{25}, an anode material under investigation for high-power applications. Before beginning her Ph.D. work, Muna performed research on cathode materials for lithium−sulfur batteries under the supervision of Dr. Brett Helms at Lawrence Berkeley National Laboratory through the Berkeley Lab Undergraduate Research (BLUR) and Science Undergraduate Laboratory Internship (SULI) DOE summer research internship programs. She graduated with a Bachelor of Science in Chemical Engineering from the University of Illinois at Chicago (UIC) in 2016.

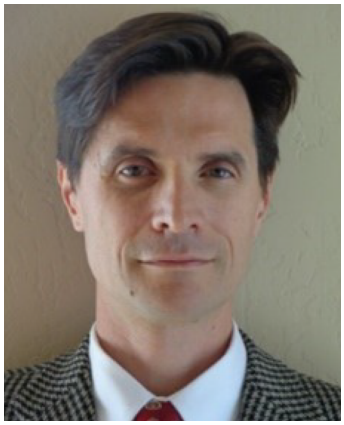

Anton Van der Ven is professor of materials at the University of California, Santa Barbara (UCSB). He studied metallurgy and applied materials science at the Katholieke Universiteit Leuven, Belgium, and obtained a Ph.D. in Materials Science at the Massachusetts Institute of Technology (MIT) in 2000. He develops and applies first-principles statistical mechanics methods and software to predict thermodynamic, kinetic, and mechanical properties of materials. He studies a wide variety of materials classes for electrochemical energy storage and high temperature structural applications.

Laurent Pilon is professor in the mechanical and aerospace engineering department at the University of California, Los Angeles (UCLA). His research group is engaged in a wide range of interdisciplinary research projects at the intersection of interfacial and transport phenomena, material science, and electrochemistry for the development of sustainable energy conversion, energy storage, and

https://doi.org/10.1021/acs.jpcc.1c10414
J. Phys. Chem. C 2022, 126, 6096−6110

energy efficiency technologies. He received a bachelor's and a master's degree in applied physics from the Grenoble Institute of Technology, France and a Ph.D. in mechanical engineering from Purdue University in 2002. More information is available at https://samueli.ucla.edu/people/laurent-pilon/.

■ ACKNOWLEDGMENTS

This work was supported as part of the Center for Synthetic Control Across Length-scales for Advancing Rechargeables (SCALAR), an Energy Frontier Research Center funded by the U.S. Department of Energy, Office of Science, Basic Energy Sciences, under Award No. DE-SC0019381.

■ REFERENCES

(1) Kim, H.; Jeong, G.; Kim, Y.-U.; Kim, J.-H.; Park, C.-M.; Sohn, H.-J. Metallic anodes for next generation secondary batteries. *Chem. Soc. Rev.* **2013**, *42*, 9011−9034.
(2) Lu, L.; Han, X.; Li, J.; Hua, J.; Ouyang, M. A review on the key issues for lithium-ion battery management in electric vehicles. *J. Power Sources* **2013**, *226*, 272−288.
(3) Shukla, A.; Kumar, T. Materials for next-generation lithium batteries. *Curr. Sci.* **2008**, *94*, 314−331.
(4) Cao, J.; Emadi, A. A new battery/ultracapacitor hybrid energy storage system for electric, hybrid, and plug-in hybrid electric vehicles. *IEEE Transactions on Power Electronics* **2012**, *27*, 122−132.
(5) Zhang, J.; Zhang, L.; Sun, F.; Wang, Z. An overview on thermal safety issues of lithium-ion batteries for electric vehicle application. *IEEE Access* **2018**, *6*, 23848−23863.
(6) Walter, M.; Kovalenko, M.; Kravchyk, K. Challenges and benefits of post-lithium-ion batteries. *New J. Chem.* **2020**, *44*, 1677−1683.
(7) Larcher, D.; Tarascon, J.-M. Towards greener and more sustainable batteries for electrical energy storage. *Nat. Chem.* **2015**, *7*, 19−29.
(8) Janek, J.; Zeier, W. A solid future for battery development. *Nature Energy* **2016**, *1*, 1−4.
(9) Dahn, J.; Haering, R. Entropy measurements on Li_xTiS_2. *Can. J. Phys.* **1983**, *61*, 1093−1098.
(10) Jiang, J.; Shi, W.; Zheng, J.; Zuo, P.; Xiao, J.; Chen, X.; Xu, W.; Zhang, J.-G. Optimized operating range for large-format $LiFePO_4$/graphite batteries. *J. Electrochem. Soc.* **2014**, *161*, A336−A341.
(11) Allart, D.; Montaru, M.; Gualous, H. Model of lithium intercalation into graphite by potentiometric analysis with equilibrium and entropy change curves of graphite electrode. *J. Electrochem. Soc.* **2018**, *165*, A380−A387.
(12) Reimers, J.; Dahn, J. Electrochemical and in situ X-ray diffraction studies of lithium intercalation in Li_xCoO_2. *J. Electrochem. Soc.* **1992**, *139*, 2091−2097.
(13) Zhang, X.; Gao, M.; Gu, Y.; Bao, H.; Li, X.; Zhou, X.; Wen, W. The Structure−Property Investigation of $Bi_{1-x}Ce_xFeO_3$ (x = 0, 0.05)−Li Battery: *In Situ* XRD and XANES Studies. *J. Phys. Chem. C* **2012**, *116*, 20230−20238.
(14) Amatucci, G.; Tarascon, J.; Klein, L. CoO_2, the end member of the Li_xCoO_2 solid solution. *J. Electrochem. Soc.* **1996**, *143*, 1114−1123.
(15) Morcrette, M.; Chabre, Y.; Vaughan, G.; Amatucci, G.; Leriche, J.-B.; Patoux, S.; Masquelier, C.; Tarascon, J. *In situ* X-ray diffraction techniques as a powerful tool to study battery electrode materials. *Electrochim. Acta* **2002**, *47*, 3137−3149.
(16) Chen, G.; Song, X.; Richardson, T. Electron microscopy study of the $LiFePO_4$ to $FePO_4$ phase transition. *Electrochemical and Solid State Letters* **2006**, *9*, A295−A298.
(17) Miller, D.; Proff, C.; Wen, J.; Abraham, D.; Bareno, J. Observation of microstructural evolution in Li battery cathode oxide particles by *in situ* electron microscopy. *Adv. Energy Mater.* **2013**, *3*, 1098−1103.
(18) Wang, H.; Jang, Y.-I.; Huang, B.; Sadoway, D.; Chiang, Y. TEM study of electrochemical cycling-induced damage and disorder in $LiCoO_2$ cathodes for rechargeable lithium batteries. *J. Electrochem. Soc.* **1999**, *146*, 473−480.
(19) Kitta, M.; Akita, T.; Tanaka, S.; Kohyama, M. Characterization of two phase distribution in electrochemically-lithiated spinel $Li_4Ti_5O_{12}$ secondary particles by electron energy-loss spectroscopy. *J. Power Sources* **2013**, *237*, 26−32.
(20) Wu, H.-L.; Huff, L.; Gewirth, A. *In situ* Raman spectroscopy of sulfur speciation in lithium−sulfur batteries. *ACS Appl. Mater. Interfaces* **2015**, *7*, 1709−1719.
(21) Hardwick, L.; Ruch, P.; Hahn, M.; Scheifele, W.; Kötz, R.; Novák, P. *In situ* Raman spectroscopy of insertion electrodes for lithium-ion batteries and supercapacitors: First cycle effects. *J. Phys. Chem. Solids* **2008**, *69*, 1232−1237.
(22) Li, H.; Mo, Y.; Pei, N.; Xu, X.; Huang, X.; Chen, L. Surface-enhanced Raman scattering study on passivating films of Ag electrodes in lithium batteries. *J. Phys. Chem. B* **2000**, *104*, 8477−8480.
(23) Baek, S.; Wyckoff, K.; Butts, D.; Bienz, J.; Likitchatchawankun, A.; Preefer, M.; Frajnkovič, M.; Dunn, B.; Seshadri, R.; Pilon, L. *Operando* Calorimetry Informs the Origin of Rapid Rate Performance in Microwave-prepared $TiNb_2O_7$ Electrodes. *J. Power Sources* **2021**, *490*, 229537.
(24) Zhang, X.-F.; Zhao, Y.; Patel, Y.; Zhang, T.; Liu, W.-M.; Chen, M.; Offer, G.; Yan, Y. Potentiometric measurement of entropy change for lithium batteries. *Phys. Chem. Chem. Phys.* **2017**, *19*, 9833−9842.
(25) Schmidt, J.; Weber, A.; Ivers-Tiffée, E. A novel and precise measuring method for the entropy of lithium-ion cells: ΔS via electrothermal impedance spectroscopy. *Electrochim. Acta* **2014**, *137*, 311−319.
(26) Thompson, A. Thermodynamics of Li intercalation batteries: Entropy measurements on Li_xTiS_2. *Physica B+C* **1981**, *105*, 461−465.
(27) Mercer, M.; Finnigan, S.; Kramer, D.; Richards, D.; Hoster, H. The influence of point defects on the entropy profiles of Lithium Ion Battery cathodes: a lattice-gas Monte Carlo study. *Electrochim. Acta* **2017**, *241*, 141−152.
(28) Hudak, N.; Davis, L.; Nagasubramanian, G. Cycling-induced changes in the entropy profiles of lithium cobalt oxide electrodes. *J. Electrochem. Soc.* **2015**, *162*, A315−A321.
(29) Jalkanen, K.; Aho, T.; Vuorilehto, K. Entropy change effects on the thermal behavior of a $LiFePO_4$/graphite lithium-ion cell at different states of charge. *J. Power Sources* **2013**, *243*, 354−360.
(30) Wang, S. Entropy and heat generation of lithium cells/batteries. *Chinese Physics B* **2016**, *25*, 010509.
(31) Zhang, Z.; Zhang, S. *Rechargeable Batteries*; Springer: New York, 2015.
(32) Bard, A.; Faulkner, L. *Electrochemical Methods Fundamentals and Applications*; John Wiley & Sons: New York, 2001.
(33) Van der Ven, A.; Bhattacharya, J.; Belak, A. Understanding Li diffusion in Li-intercalation compounds. *Acc. Chem. Res.* **2013**, *46*, 1216−1225.
(34) Van der Ven, A.; Wagemaker, M. Effect of surface energies and nano-particle size distribution on open circuit voltage of Li-electrodes. *Electrochemistry communications* **2009**, *11*, 881−884.
(35) Moran, M.; Bailey, M.; Boettner, D.; Shapiro, H. *Fundamentals of Engineering Thermodynamics*; John Wiley & Sons: New York, 2018.
(36) Chase, M. W. NIST-JANAF thermochemical tables. *J. Phys. Chem. Ref. Data, Monograph 9* **1998**, 1.
(37) Lu, W.; Belharouak, I.; Liu, J.; Amine, K. Thermal properties of $Li_{4/3}Ti_{5/3}O_4/LiMn_2O_4$ cell. *J. Power Sources* **2007**, *174*, 673−677.
(38) Ohzuku, T.; Ueda, A. Solid-state redox reactions of $LiCoO_2$ (R3m) for 4 V secondary lithium cells. *J. Electrochem. Soc.* **1994**, *141*, 2972−2977.
(39) Wang, J. Model for lithium intercalation into TiS_2. *Solid State Ionics* **1990**, *40*, 548−552.
(40) Whittingham, M. Ultimate limits to intercalation reactions for lithium batteries. *Chem. Rev.* **2014**, *114*, 11414−11443.
(41) Ceder, G. A derivation of the Ising model for the computation of phase diagrams. *Comput. Mater. Sci.* **1993**, *1*, 144−150.

https://doi.org/10.1021/acs.jpcc.1c10414
J. Phys. Chem. C 2022, 126, 6096−6110

(42) Van der Ven, A.; Thomas, J. C.; Puchala, B.; Natarajan, A. R. First-principles statistical mechanics of multicomponent crystals. *Annu. Rev. Mater. Res.* **2018**, *48*, 27−55.
(43) Van der Ven, A.; Deng, Z.; Banerjee, S.; Ong, S. P. Rechargeable alkali-ion battery materials: theory and computation. *Chem. Rev.* **2020**, *120*, 6977−7019.
(44) van de Walle, A.; Ceder, G. The effect of lattice vibrations on substitutional alloy thermodynamics. *Rev. Mod. Phys.* **2002**, *74*, 11−45.
(45) Reynier, Y.; Graetz, J.; Swan-Wood, T.; Rez, P.; Yazami, R.; Fultz, B. Entropy of Li intercalation in Li_xCoO_2. *Phys. Rev. B* **2004**, *70*, 174304.
(46) Natarajan, A.; Thomas, J.; Puchala, B.; Van der Ven, A. Symmetry-adapted order parameters and free energies for solids undergoing order-disorder phase transitions. *Phys. Rev. B* **2017**, *96*, 134204.
(47) Wallace, D. *Thermodynamics of Crystals*; Dover: Mineola, NY, 1998.
(48) Van der Ven, A.; Aydinol, M.; Ceder, G.; Kresse, G.; Hafner, J. First-principles investigation of phase stability in Li_xCoO_2. *Phys. Rev. B* **1998**, *58*, 2975.
(49) Kaufman, J. L.; Vinckevičiūtė, J.; Krishna Kolli, S.; Goiri, J.; Van der Ven, A. Understanding intercalation compounds for sodium-ion batteries and beyond. *Philosophical Transactions of the Royal Society A* **2019**, *377*, 20190020.
(50) Pal, S. Phonon Dispersion in Lithium. *Phys. Rev. B* **1970**, *2*, 4741−4742.
(51) Chen, M.-H.; Puchala, B.; Van der Ven, A. High-temperature stability of δ'-ZrO. *Calphad* **2015**, *51*, 292−298.
(52) Rhein, R. K.; Dodge, P. C.; Chen, M.-H.; Titus, M. S.; Pollock, T. M.; Van der Ven, A. Role of vibrational and configurational excitations in stabilizing the $L1_2$ structure in Co-rich Co-Al-W alloys. *Phys. Rev. B* **2015**, *92*, 174117.
(53) Zhou, F.; Maxisch, T.; Ceder, G. Configurational electronic entropy and the phase diagram of mixed-valence oxides: the case of Li_xFePO_4. *Phys. Rev. Lett.* **2006**, *97*, 155704.
(54) Decolvenaere, E.; Levin, E.; Seshadri, R.; Van der Ven, A. Modeling magnetic evolution and exchange hardening in disordered magnets: The example of $Mn_{1-x}Fe_xRu_2Sn$ Heusler alloys. *Physical Review Materials* **2019**, *3*, 104411.
(55) Kitchaev, D. A.; Schueller, E. C.; van der Ven, A. Mapping skyrmion stability in uniaxial lacunar spinel magnets from first principles. *Phys. Rev. B* **2020**, *101*, 054409.
(56) Zuo, J. L.; Kitchaev, D.; Schueller, E. C.; Bocarsly, J. D.; Seshadri, R.; van der Ven, A.; Wilson, S. D. Magnetoentropic mapping and computational modeling of cycloids and skyrmions in the lacunar spinels GaV_4S_8 and GaV_4Se_8. *Physical Review Materials* **2021**, *5*, 054410.
(57) Stern, E. A. Rigid-band model of alloys. *Phys. Rev.* **1967**, *157*, 544−551.
(58) Kaufman, J. L.; Van der Ven, A. Na_xCoO_2 phase stability and hierarchical orderings in the O3/P3 structure family. *Physical Review Materials* **2019**, *3*, 015402.
(59) Van der Ven, A.; Thomas, J. C.; Xu, Q.; Swoboda, B.; Morgan, D. Nondilute diffusion from first principles: Li diffusion in Li_xTiS_2. *Phys. Rev. B* **2008**, *78*, 104306.
(60) Whittingham, M. Lithium batteries and cathode materials. *Chem. Rev.* **2004**, *104*, 4271−4302.
(61) Thomas, K. E.; Newman, J. Heats of mixing and of entropy in porous insertion electrodes. *J. Power Sources* **2003**, *119*, 844−849.
(62) Verde, M.; Baggetto, L.; Balke, N.; Veith, G.; Seo, J.; Wang, Z.; Meng, Y. Elucidating the phase transformation of $Li_4Ti_5O_{12}$ lithiation at the nanoscale. *ACS Nano* **2016**, *10*, 4312−4321.
(63) Laffont, L.; Delacourt, C.; Gibot, P.; Wu, M.; Kooyman, P.; Masquelier, C.; Tarascon, J. Study of the $LiFePO_4/FePO_4$ two-phase system by high-resolution electron energy loss spectroscopy. *Chem. Mater.* **2006**, *18*, 5520−5529.
(64) Dedryvere, R.; Maccario, M.; Croguennec, L.; le Cras, F.; Delmas, C.; Gonbeau, D. X-ray photoelectron spectroscopy investigations of carbon-coated Li_xFePO_4 materials. *Chem. Mater.* **2008**, *20*, 7164−7170.
(65) Castro, L.; Dedryvere, R.; el Khalifi, M.; Lippens, P.-E.; Bréger, J.; Tessier, C.; Gonbeau, D. The spin-polarized electronic structure of $LiFePO_4$ and $FePO_4$ evidenced by in-lab XPS. *J. Phys. Chem. C* **2010**, *114*, 17995−18000.
(66) Levi, M.; Levi, E.; Aurbach, D. The mechanism of lithium intercalation in graphite film electrodes in aprotic media. Part 2. Potentiostatic intermittent titration and in situ XRD studies of the solid-state ionic diffusion. *J. Electroanal. Chem.* **1997**, *421*, 89−97.
(67) Park, J.; Park, S.; Won, Y. *In situ* XRD study of the structural changes of graphite anodes mixed with SiO_x during lithium insertion and extraction in lithium ion batteries. *Electrochim. Acta* **2013**, *107*, 467−472.
(68) Pande, V.; Viswanathan, V. Robust high-fidelity DFT study of the lithium-graphite phase diagram. *Physical Review Materials* **2018**, *2*, 125401.
(69) Reynier, Y.; Yazami, R.; Fultz, B. The entropy and enthalpy of lithium intercalation into graphite. *J. Power Sources* **2003**, *119*, 850−855.
(70) Reynier, Y.; Yazami, R.; Fultz, B. Thermodynamics of lithium intercalation into graphites and disordered carbons. *J. Electrochem. Soc.* **2004**, *151*, A422−A426.

https://doi.org/10.1021/acs.jpcc.1c10414
J. Phys. Chem. C 2022, 126, 6096−6110